

# Lithographic production of vertically aligned CNT strain sensors for integration in soft robotic microactuators

B. Gorissen, E. Milana, D. Reynaerts, M. De Volder

**Abstract**— This paper reports on a piezoresistive strain sensor that uses vertically aligned carbon nanotube (CNT) filler elements which are embedded in a rubber matrix. Compared to previously used conductive filler elements, vertical CNTs can be patterned using lithography, making it possible to scale down the sensor footprint into the micrometer range. This technological advancement is instrumental for developing intelligent soft microrobots with embedded flexible sensors. We compare vertical CNTs and carbon black as filler elements, where newly developed lithographic production techniques are applied to shape a generic strain sensor topology that is compatible with the majority of planar inflatable microactuators. This research shows a significant improvement in sensor linearity by using vertical CNTs as filler elements over carbon black. Further, a lithographically fabricated strain sensor has been successfully embedded in an elastic inflatable bending microactuator with outer dimensions of  $5.5 \times 1 \times 0.06 \text{ mm}^3$ . The full lithographic production process to create this actuator is described in this paper, together with its characterization under a static pressure input.

## I. INTRODUCTION

Soft robotic actuators may very well revolutionize 21<sup>st</sup> century robotic systems. These actuators are anticipated to take prominent roles in delicate tasks where classic robots fail, such as in minimally invasive surgery [1] and man-machine interactions. Their high compliance renders them inherently safe in contact with more rigid bodies: when an unwanted collision occurs between a soft actuator and a more rigid object, the soft structure will absorb the majority of the released energy. In literature [2, 3], applications listed for soft robots are most often found in medicine with special interest in the field of microsurgery. These applications include catheterization procedures, where bending actuators are used to steer inside the human venous system [4]; ophthalmological procedures, where soft actuators are integrated in a tool for retinal pigment epithelium transplantation [5] and microtweezers for the manipulation of single cell aggregates [6]. These applications can all be characterized by overall tool dimensions in the order of a few millimeters and smaller.

While production processes have been developed to produce these micro-sized actuators based on soft lithography [7], MeME-X [4], stereolithography [8] or full lithography [9], there still remains a bottleneck in producing highly flexible sensors that can be integrated in soft microrobots. Large soft robots sometimes use sensors based on conductive paste [10] or fluid resistivity [11, 12], but these sensors are not compatible with the aforementioned production processes

used for fabricating soft microrobots. This is because they all need manual production or assembly steps. This barrier hampers the development of soft intelligent microrobots, where sensory information closes the feedback loop and makes it possible for them to adapt to the environment. While sensor integration is currently being pursued in the field of large scale soft robots [13], few research attempts have been made on a microscale. The solution that is proposed in this paper is to use conductive filler elements in a silicone rubber matrix, to form a new composite material. When these filler elements are placed in a well-designed path, strains can be registered that correlate to the overall actuator deformation. Since the filler elements are embedded in a highly flexible matrix, the overall sensor retains this flexibility, making it possible to register large strains that are typical in the field of soft robotics. Further, since previous research showed that silicone rubber structures out of PDMS can be patterned using lithographic techniques, it is highly likely that this new conductive composite can also be patterned with micrometer accuracy [9], opening the way for the envisioned microscale applications.

In literature, two main filler elements are used to render PDMS conductive: silver and carbon based particles. These elements come in different forms (flakes, spheroidal particles, nanotubes, foam), with different dielectric and piezoresistive properties as summarized in table 1. From this table it can be concluded that conductivity is higher for silver based filler elements, however the percolation threshold is far lower for carbon based fillers, meaning that less material is needed to render the PDMS material conductive. Further, a comparative study between silver and carbon filler elements by Niu et al. [14] concluded that silver particles show a large conductivity hysteresis, which is undesirable in strain sensor applications, especially when aiming at closed loop control. Therefore, this paper will use carbon based materials as filler elements, where a comparative study will be performed between round carbon black fillers and vertically aligned carbon nanotube ‘forests’ [15]. We developed a lithographic production process for both types of carbon particles, and subsequently tested their properties in a uniaxial strain setup. Further, we demonstrate that these sensors can be embedded in an elastic inflatable actuator with bending deformation that is fabricated using lithographic production processes. This integration is realized without the use of manual alignment or transfer steps. Finally, this actuator with embedded sensor is tested to show the resistance change vs bending deformation.

Benjamin Gorissen, Edoardo Milana, Michael De Volder and Dominiek Reynaerts are with the Department of Mechanical Engineering, University of Leuven, and also member of Flanders Make, Heverlee, Belgium.

(Corresponding author is Benjamin Gorissen; e-mail: benjamin.gorissen@kuleuven.be).

Michael De Volder is also affiliated with the Institute for Manufacturing, Department of Engineering, University of Cambridge, Cambridge, UK

TABLE 1. OVERVIEW OF KEY PUBLICATIONS ON FILLER ELEMENTS TO RENDER PDMS CONDUCTIVE. \*: ALIGNED CNTS

Filler element	Filler shape	Filler size [ $\mu\text{m}$ ]	Weight percent	Conductivity [S/m]	Ref.
Silver	round	2	72-74%	$10^4$	[16]
	round	2-3.5	70%	$10^2$	[17]
	round	1-2	83%	$10^4$	[14]
	flake	9	80%	$1.4 \times 10^5$	[18]
Carbon	round	0.04-0.1	26%	$2.5 \times 10^2$	[14]
	tube*	?	?	$10-10^2$	[19]
	tube	$\text{\O}0.2 \times 5$	10-15%	$2 \times 10^2$	[20]
	tube	$\text{\O}0.04$	15%	6.3	[21]
	foam	?	0.5%	$10^3$	[22]

## II. CARBON-PDMS STRAIN SENSOR

### A. Fabrication

Two different lithographic fabrication processes have been developed for integrating carbon black or vertically aligned CNT filler elements in a PDMS matrix. Both processes can be used to shape sensors that are compatible with planar inflatable actuator designs as depicted in fig. 1, where A shows the production process using carbon black filler elements and B using vertically aligned CNTs. Both production processes are explained in the following paragraphs.

A commercially available type of carbon black (Vulcan XC72R) is used in this research to render PDMS conductive. To achieve a good dispersion of filler elements in the rubber matrix, agglomerates are broken down in a first step by dissolving them in tetrahydrofuran (THF) in a 10:1 ratio, after which PDMS (Sylgard 184) base polymer is added and thoroughly mixed by hand. This mixture is placed on a hot plate ( $60^\circ\text{C}$ ) overnight for THF to evaporate, leaving a mixture of PDMS base polymer with dispersed carbon black. After adding PDMS curing agent in a 1:10 ratio, and mixing by hand, the mixture can be molded. The mold is fabricated by patterning a photoresist layer (AZ4562) to form the sensor's planar topology (Fig. 1 A1). After coating with a demolding agent (TFCOS), the viscous uncured carbon black PDMS (CPDMS) is worked in by hand, and excess material is scraped off. After curing at  $90^\circ\text{C}$ , the patterned mold is dissolved using acetone, leaving a bare CPDMS strain sensor on a silicon support wafer. Lastly, the sensor is embedded in PDMS using spin coating and subsequent curing. Although this production process uses a manual production step, where excess PDMS is scraped off, a lithographic PDMS patterning technique (eg. [9]) could be used to shape the sensor structure, which would result in a structure equivalent to the one that was achieved with the presented micromolding technique. This would also make it possible to downscale sensor dimensions.

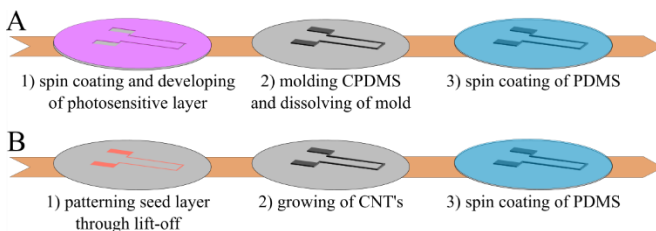


Figure 1 Lithographic production process for a piezoresistive strain sensor embedded in PDMS, using A) carbon black and B) vertically aligned CNTs as filler elements.

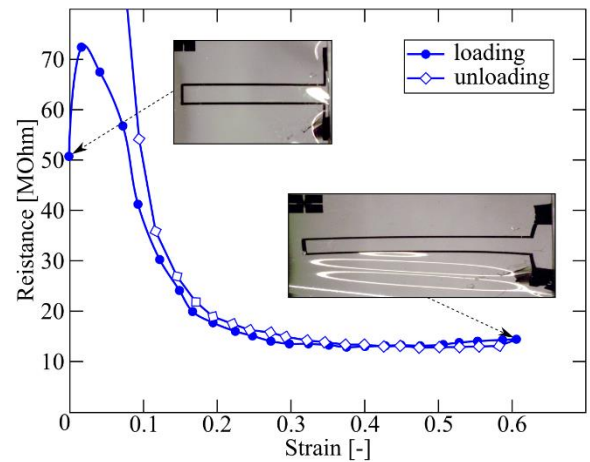


Figure 2 Resistance vs. strain for a sensor with carbon black filler elements. Inset pictures show sensor deformation.

Vertically aligned CNT sensors are fabricated using a different lithographic process, depicted in fig. 1B. First, a catalyst seed layer (10nm of  $\text{Al}_2\text{O}_3$  and 1nm of Fe) is deposited by e-beam evaporation and patterned using a lift-off process. Next, CNTs are grown at atmospheric pressure in a horizontal tube furnace with flows of 100/400/100sccm of respectively  $\text{C}_2\text{H}_4/\text{H}_2/\text{He}$  at  $775^\circ\text{C}$  for 5 minutes. This resulted in a vertically oriented CNT forest with approximate height of  $500\mu\text{m}$ , where height and forest density can be altered by tuning parameter values. After PDMS (Sylgard 184 in 10:1 ratio) is poured on top, the substrate is degassed in vacuum to fully flood the CNT forest. Lastly, spincoating, full curing ( $70^\circ\text{C}$ ) and peeling resulted in the same sensor architecture as the CPDMS sensor.

### B. Uniaxial testing

The two strain sensors are tested using a uniaxial strain setup, where incremental displacements are imposed to a PDMS sheet with the embedded sensors. Displacements are imposed by a linear stage driven by a micrometer screw, however the actual strain is measured using a digital microscope (Zeiss stereo discovery V20) with measurement software. The strain sensors are electrically connected to a digital multimeter (Keithley 2000). In order not to influence the measurements, the connection to the sensor is realized outside of the strained zone. In this way, the contact resistance between sensor and electrical leads are minimally influenced by the imposed strain.

For the CPDMS strain sensor, the uniaxial test results are shown in fig. 2. During this test, immediately after a strain increment is imposed, the resistance increased rapidly, while subsequently stabilizing at a lower resistance value. Measurement points in fig. 2 are taken after the resistance settled at a constant value. This time-dependent behavior has also been previously reported in the literature[23, 24], and has been attributed to resistance relaxation due to the viscoelastic properties of PDMS and van der Waals forces that reconnect carbon black chains after loading increments. When loading the strain sensor, a first step increase in resistance is observed, followed by a decrease until a strain of 40%. This behavior will be discussed in the discussion section, and is believed to originate from nonlinear realignment of carbon black particles in the PDMS matrix.

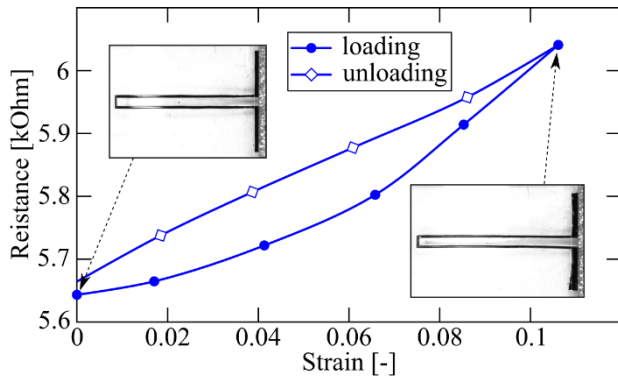


Figure 3 Resistance vs. strain for a sensor with vertically aligned CNT filler elements. Inset pictures show sensor deformation.

For vertically aligned CNT filler elements, the strain sensor results are shown on figure 3, for strains up to 10%. Because strain is applied perpendicular to the growth direction of the CNT forest, the orientation of the CNTs remains constant during straining, which leads to a more or less linear input-output relation. The changes in resistance can be linked to two factors: (1) a geometrical effect where with increased strain the length of the conductive paths is increased and the cross-sectional area is decreased; (2) a change in resistivity that is caused by an increase in average distance between carbon nanotubes when strained, where electrical contact will be lost between some of them.

When comparing carbon black to vertically aligned CNT filler elements over the same strain range (0-10%), a more linear behavior of the latter can be observed, together with a general decrease in magnitude of resistance. Therefore vertical CNTs are chosen to be embedded in a planar inflatable actuator. A disadvantage however is the larger observed hysteresis for the CNT based sensors.

### III. EMBEDDED STRAIN SENSOR

To demonstrate the application of this technology in the field of soft microrobotics, a strain sensor is embedded in a planar bending microactuator, that has been extensively described in literature [25] and of which the topology is shown in fig. 4. On a larger scale, this planar actuator design is also known by the name PneuNets [26]. Essentially this type of actuator consists of an inflatable central void (hatched in fig.4) that is asymmetrically surrounded by two sheets with different stiffnesses. The strain sensor, in black, is embedded around the central void. Both electrical and pneumatic connections are located at the region of the actuator that is clamped, to ensure that they deform as little as possible during actuation.

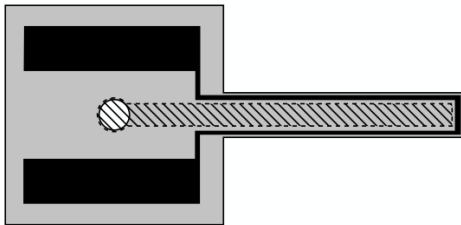


Figure 4 Topology of the developed bending actuator with embedded strain sensor. The extent of the actuator is shown in grey, the inflatable void in hatched lines and the conductive path in black.

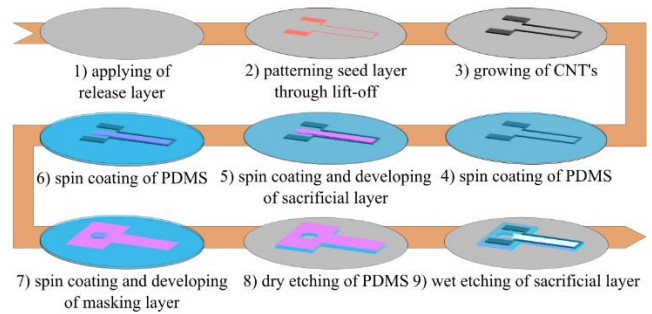


Figure 5 Lithographic production process for fabricating elastic inflatable bending microactuators with embedded CNT strain sensor that omits manual alignment or transfer steps.

### A. Fabrication

To fabricate these bending actuators, a new lithographic process flow has been developed that fully omits manual positioning and transfer steps, as can be seen in fig. 5. In a first step, a 70nm TiN release layer is deposited to easily remove the actuator by peeling in a last step. In the three subsequent steps, the strain sensor with vertically aligned CNTs is made by the same process as explained in the previous paragraphs, where in step 4 the PDMS layer (ratio 10:1) is spincoated at 3000 rpm to have a thickness of  $\approx 37\mu\text{m}$ . Further, a sacrificial layer (AZ 4562) is deposited and patterned to create the inflatable void together with the internal pressure supply channel. The layer is spincoated at 2000 rpm, resulting in a thickness of  $\approx 10\mu\text{m}$ . To seal the void, another layer of PDMS (ratio 10:1) is spincoated at a speed of 6000 rpm, resulting in an average thickness of  $\approx 23\mu\text{m}$ . As such, all the internal structures of the actuator are asymmetrically encapsulated where asymmetry is essential for achieving the bending deformation.

To define the outer contours of the actuator, PDMS is locally removed using reactive ion etching (RIE), a process that is explained in detail in [9]. To protect the underlying structures a LOR\_30B/SU8\_2050 masking layer is spin coated and patterned, where its geometry is shown in grey in fig. 4. SU8 acts as dry etch mask that is resisting the directional etching step, while LOR acts as a release layer between PDMS and SU8. PDMS etching is performed using a 1:4 volume ratio of  $\text{O}_2$  to  $\text{SF}_6$ , which is a near optimal ratio for the fast etching of PDMS [27]. At a pressure of 150mtorr and a RIE power of 300W, etching is performed in 9 consecutive steps of 10 minutes each, to ensure that PDMS is fully etched away where no masking SU8 layer is present. After etching, the SU8 layer is removed through lift-off by dissolving the sacrificial LOR layer underneath using a developer (OPD 5262). The RIE process also opens the pressure connection hole that is shown in white with black hatched lines in fig. 4. This hole is needed for both pressurization of the actuator and for wet etching of the sacrificial layer between both PDMS layer that forms the inflatable void, and which is shown in hatched lines in fig. 4. This last wet etching step is performed using acetone, which introduced a temporarily light amount of swelling of the PDMS polymer that disappears after acetone evaporation. The actuator is completed after it is peeled off from the silicon wafer substrate. A finished actuator is shown in fig. 6 with external dimension of  $5.5 \times 1 \times 0.06 \text{mm}^3$  and where the inflatable central void has dimensions of  $5 \times 0.5 \times 0.01 \text{mm}^3$ .

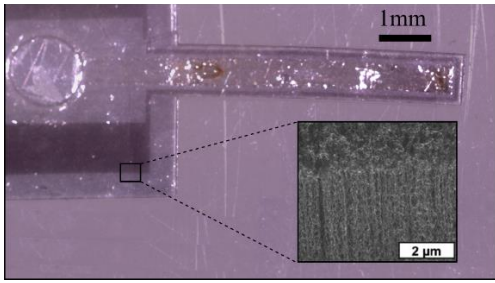


Figure 6 Top view of the developed bending inflatable microactuator with embedded CNT strain sensor. Inset picture shows a scanning electron microscopic image of the CNTs.

### B. Testing

The manufactured inflatable elastic microactuator is characterized using a test setup where a stepwise quasi-static input pressure is applied and output resistance is registered using a digital multimeter (Keithley 2000). Simultaneously, images of the deformation are taken using a digital microscope (Zeiss stereo discovery V20). Electrical connection to the internal strain sensor is made by means of pressing it against two mutually isolated electrical conductor blocks where a pressure supply hole is foreseen to create the pneumatic connection.

The result of this test in terms of relative resistance change to input pressure can be seen in fig. 7. This shows that up to a pressure of 30kPa, there is a linear relation between both. However, at larger pressures, this linear relation stops holding. When looking at the deformations that appear at these pressure levels, as are shown on figure 8, it can be seen that below a pressure of 40kPa only limited bending deformations are displayed. While suddenly, at a pressure of 50kPa, the actuator shows a large deformation. Although this large deformation is accompanied by large strains, an increase in sensor resistance, as is expected according to fig. 3, is not registered, as can be seen in fig.7. This unexpected nonlinear behavior will be discussed in the following section. Further, it should be mentioned that due to residual stresses of the manufacturing process, the actuator shows an initial bending deformation that is counteracted by the actuated bending deformation.

Although there is no linear relation between pressure input and sensor output over the entire input range, a distinctive correlation between both can be seen. Further, when only limited deformations are needed, the registered linear relation between 0 and 30kPa can be used for feedback control.

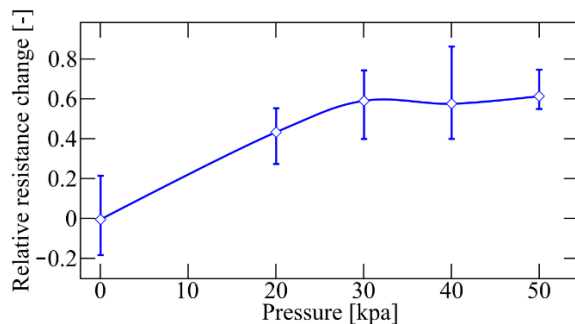


Figure 7 Relative resistance change of the embedded CNT strain sensor vs input pressure of the bending microactuator, where data is acquired from three measurement cycles, where error bars indicate measured extrimities.

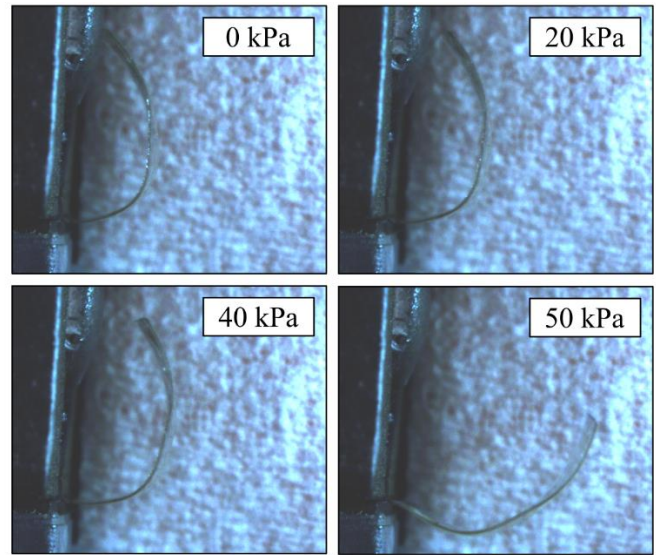


Figure 8 Registered deformation of the soft robotic bending microactuator with an integrated CNT strain sensor, subjected to an internal pressure

### DISCUSSION

The nonlinear resistance versus strain behavior of the carbon black PDMS composite material, shown on figure 2, is induced by two phenomena: a change in material resistivity and a geometrical contribution where the conductive path is elongated and narrowed in cross-section. While the geometrical effect changes linearly with strain, the origin of the nonlinear behavior can be found in the movement of carbon black particles when the surrounding PDMS matrix is strained. A possible explanation is given by Yamaguchi et al. [28]. Initial straining of a rubber material that contains highly branched carbon filler elements like Vulcan XC72R, causes the carbon black agglomerates to break down into smaller aggregates. As such, electrical connections are broken, resulting in an increase in resistivity. Loading the sample even further will impose a rotation onto these aggregates and causing them to form new electrical connections, and thus lowering the resistivity. After this realignment process, the carbon black particle orientation remains constant and resistivity changes are dominated by an increased particle spacing.

The uniaxial test of vertically aligned CNT filler elements showed a limited gauge factor (ratio of relative resistance change to strain) of 0.65. This is most likely caused by the high density of the CNT forest, where few electrical connections are broken upon loading and change in resistance is dominated by the geometrical effect instead of a changing material resistivity. As suggested in literature [29], reducing the amount of CNTs will increase sensitivity drastically. However care should be taken to still remain above the percolation threshold at all times during stretching.

The uniaxial test setup has been designed to decouple strain from the electrical connection, which resulted in a linear strain versus resistance behavior for the CNT based strain sensor, as is shown in fig. 3. This decoupling has not been implemented in the electrical connection for the embedded sensor, where the fluidic connection (white with hatched black lines in fig. 4) is located in between the electrical connections

(black squares in fig. 4). This most likely lays at the origin of the resistance flattening as is shown on the graph in fig. 7. As the input pressure increases, the electrical connection zones are pushed against the conductor blocks, resulting in a more conformal contact with the CNTs and an overall decrease in contact resistance. For further developments of this sensor in soft robotic applications, it is essential that the electrical connection to the embedded CNTs is not influenced by internal pressure loading or by external influences. To do so, the electrical connection should be made outside of the force loop of the actuator, as such that during loading, the connection is always subjected to the same mechanical boundary conditions.

Further, the electrical connection in this work has been done by means of clamping it against a conductor, which is prone to variation under external forces. In literature, solutions are found where electrodes are adhered to the CNT interface using conductive glue [19]. Another solution is to only partially peel the PDMS composite form the support wafer during fabrication, making electrical connections to the CNTs via the patterned conductive layer that is used as a seed layer for growing the CNTs. This could be implemented by slightly altering the lithographic process flow of fig. 5.

According to the production process, the strain sensor is embedded inside the thick layer of the actuator. When inflating, the bending deformation is directed towards the side with the highest bending stiffness [7], to be the thick layer in this case. This thick layer will undergo a compression due to the bending deformation and an axial elongation due to the axial component of the pressure [30], where these two will partially cancel each other out. As such, the sensor is located in a less strained part of the actuator. Better would be to locate the sensor in the thin layer of the actuator, where the elongation due to the axial component of pressure is increased by tensional stresses due to the bending deformation. This can be implemented in the production process by altering the spincoating speeds in step 4 (faster) and 6 (slower) of fig. 5, exchanging thin and thick layer and thus flipping asymmetry.

When comparing fig. 2 to fig. 3, the increased linearity is caused by loading the embedded CNT forest orthogonally with respect to its growth direction, avoiding the nonlinear mechanism of rotation and realignment of conductive particles. To maintain the orthogonal loading direction in the case of a bending actuator is relatively easy since bending deformations are characterized by large axial strains in the actuator at the bottom and top layer, justifying the line-shaped sensor path of fig. 4. For other types of actuators with different deformations, the placement of the CNTs becomes more intricate since large unidirectional deformations of the sensor are required. For instance, conductive paths should be placed under  $45^\circ$  with the longitudinal axis of twisting actuators with a circular cross section [31], because a pure torsional deformation is characterized by large tensional stresses that are oriented under  $45^\circ$  in a circular shell. For more intricate deformations, an intensive numerical study of principal strains in the structures is advised, in order to maximize sensor linearity with respect to the overall deformation.

## CONCLUSION

In this paper, a uniaxial strain sensor is proposed that is fully compatible with existing lithographic production techniques to fabricate planar inflatable soft robotic actuators with dimension in the micrometer range. The developed sensor consists of a patterned path of vertically grown CNTs, embedded in a silicone rubber that changes its resistivity when being stretched. Compared to other conductive filler elements, vertically aligned CNTs exhibit a relatively linear strain versus resistance characteristic due to the linear mechanism of increasing distance between individual CNTs under tension. This concept has been elaborated in this paper where a stand-alone CNT strain sensor has been fabricated that shows a gauge factor of 0.65 when tested using a uniaxial strain setup.

Furthermore, this strain sensor has been embedded in an elastic inflatable bending actuator with outer dimensions of  $5.5 \times 1 \times 0.06 \text{ mm}^3$ . A fully lithographic production process has been developed avoiding manual alignment or transfer steps. As such, the dimensions of 'intelligent' actuators can be downscaled into the micrometer range, opening up the implementation of feedback control in soft actuators at smaller scales than previously possible. The fabricated actuator was subjected to a stepwise increasing quasi-static pressure input while simultaneously registering actuator deformation and sensor resistance, showing a good correlation between pressure input and output resistance, being linear for small deformations.

## ACKNOWLEDGMENT

This research is supported by the Fund for Scientific Research-Flanders (FWO) and the European Research Council (ERC starting grant HIENA).

## REFERENCES

- [1] D. Rus, M.T. Tolley, Design, fabrication and control of soft robots, *Nature* 521(7553) (2015) 467-475.
- [2] B. Gorissen, D. Reynaerts, S. Konishi, K. Yoshida, J.-W. Kim, M. De Volder, Elastic Inflatable Actuators for Soft Robotic Applications, *Advanced Materials* 29(43) (2017) 1604977.
- [3] M. Cianchetti, T. Ranzani, G. Gerboni, T. Nanayakkara, K. Althoefer, P. Dasgupta, A. Menciassi, Soft Robotics Technologies to Address Shortcomings in Today's Minimally Invasive Surgery: The STIFF-FLOP Approach, *Soft Robotics* 1(2) (2014) 122-131.
- [4] M. Ikeuchi, K. Ikuta, Ieee, Development of Pressure-Driven Micro Active Catheter using Membrane Micro Emboss Following Excimer Laser Ablation (MeME-X) Process, *IEEE International Conference on Robotics and Automation, Kobe, JAPAN, 2009*, pp. 4358-4361.
- [5] M. Tokida, T. Obara, M. Takahashi, M. Yamato, S. Konishi, Ieee, INTEGRATION OF CELL SHEET SUCKING AND TACTILE SENSING FUNCTIONS TO RETINAL PIGMENT EPITHELIUM TRANSPLANTATION TOOL, *23rd IEEE International Conference on Micro Electro Mechanical Systems (MEMS 2010), Hong Kong, PEOPLES R CHINA, 2010*, pp. 316-319.
- [6] S. Konishi, S. Shimomura, S. Tajima, Y. Tabata, Implementation of soft microfingers for a hMSC aggregate manipulation system, *Microsystems & Nanoengineering* 2 (2016) 15048.
- [7] O.C. Jeong, S. Konishi, All PDMS pneumatic microfinger with bidirectional motion and its application, *Journal of Microelectromechanical Systems* 15(4) (2006) 896-903.
- [8] H.-W. Kang, I.H. Lee, D.-W. Cho, Development of a micro-bellows actuator using micro-stereolithography technology, *Microelectronic Engineering* 83(4-9) (2006) 1201-1204.

- [9] B. Gorissen, C. Van Hoof, D. Reynaerts, M. De Volder, SU8 etch mask for patterning PDMS and its application to flexible fluidic microactuators, *Microsystems & nanoengineering* 2 (2016).
- [10] K. Kure, T. Kanda, K. Suzumori, S. Wakimoto, Flexible displacement sensor using injected conductive paste, *Sensors and Actuators a-Physical* 143(2) (2008) 272-278.
- [11] S. Kusuda, S. Sawano, S. Konishi, Fluid-resistive bending sensor having perfect compatibility with flexible pneumatic balloon actuator, 2007 20th IEEE International Conference on Micro Electro Mechanical Systems - MEMS '07 (2007) 615-18.
- [12] S. Russo, T. Ranzani, H. Liu, S. Nefti-Meziani, K. Althoefer, A. Menciasci, Soft and Stretchable Sensor Using Biocompatible Electrodes and Liquid for Medical Applications, *Soft Robotics* 2(4) (2015) 146-154.
- [13] G. Gerboni, A. Diodato, G. Ciuti, M. Cianchetti, A. Menciasci, Feedback Control of Soft Robot Actuators via Commercial Flex Bend Sensors, *Ieee-Asme Transactions on Mechatronics* 22(4) (2017) 1881-1888.
- [14] X. Niu, S. Peng, L. Liu, W. Wen, P. Sheng, Characterizing and patterning of PDMS-based conducting composites, *Advanced Materials* 19(18) (2007) 2682-+.
- [15] M.F.L. De Volder, D.O. Vidaud, E.R. Meshot, S. Tawfick, A.J. Hart, Self-similar organization of arrays of individual carbon nanotubes and carbon nanotube micropillars, *Microelectronic Engineering* 87(5-8) (2010) 1233-1238.
- [16] H. Cong, T. Pan, Ieee, Microfabrication of Conductive PDMS on Flexible Substrates for Biomedical Applications, 2009 4th Ieee International Conference on Nano/Micro Engineered and Molecular Systems, Vols 1 and 2 (2009) 731-734.
- [17] H. Cong, T. Pan, Photopatternable conductive PDMS materials for microfabrication, *Advanced Functional Materials* 18(13) (2008) 1912-1921.
- [18] J.C. Agar, K.J. Lin, Z. Rongwei, J. Durden, M. Kyoung-Sik, C.P. Wong, Novel PDMS(silicone)-in-PDMS(silicone): Low Cost Flexible Electronics without Metallization, *Proceedings IEEE 60th Electronic Components and Technology Conference (ECTC 2010)* (2010) 1226-30.
- [19] Y.J. Jung, S. Kar, S. Talapatra, C. Soldano, G. Viswanathan, X.S. Li, Z.L. Yao, F.S. Ou, A. Avadhanula, R. Vajtai, S. Curran, O. Nalamasu, P.M. Ajayan, Aligned carbon nanotube-polymer hybrid architectures for diverse flexible electronic applications, *Nano Letters* 6(3) (2006) 413-418.
- [20] J. Engel, J. Chen, N. Chen, S. Pandya, C. Liu, Ieee, Multi-walled carbon nanotube filled conductive elastomers: Materials and application to micro transducers, 19th IEEE International Conference on Micro Electro Mechanical Systems (MEMS 2006), Istanbul, TURKEY, 2006, pp. 246-249.
- [21] C.-X. Liu, J.-W. Choi, Patterning conductive PDMS nanocomposite in an elastomer using microcontact printing, *Journal of Micromechanics and Microengineering* 19(8) (2009).
- [22] Z. Chen, W. Ren, L. Gao, B. Liu, S. Pei, H.-M. Cheng, Three-dimensional flexible and conductive interconnected graphene networks grown by chemical vapour deposition, *Nature Materials* 10(6) (2011) 424-428.
- [23] T. Ding, L. Wang, P. Wang, Changes in electrical resistance of carbon-black-filled silicone rubber composite during compression, *Journal of Polymer Science Part B-Polymer Physics* 45(19) (2007) 2700-2706.
- [24] J. Kost, A. Foux, M. Narkis, QUANTITATIVE MODEL RELATING ELECTRICAL-RESISTANCE, STRAIN, AND TIME FOR CARBON-BLACK LOADED SILICONE-RUBBER, *Polymer Engineering and Science* 34(21) (1994) 1628-1634.
- [25] B. Gorissen, R. Donose, D. Reynaerts, M. De Volder, Flexible pneumatic micro-actuators: analysis and production, *Procedia Engineering* 25 (2011) 681-684.
- [26] F. Ilievski, A.D. Mazzeo, R.E. Shepherd, X. Chen, G.M. Whitesides, *Soft Robotics for Chemists*, *Angewandte Chemie-International Edition* 50(8) (2011) 1890-1895.
- [27] D. Szmigiel, K. Domanski, P. Prokaryn, P. Grabiec, Deep etching of biocompatible silicone rubber, *Microelectronic Engineering* 83(4-9) (2006) 1178-1181.
- [28] K. Yamaguchi, J.J.C. Busfield, A.G. Thomas, Electrical and mechanical behavior of filled elastomers. I. The effect of strain, *Journal of Polymer Science Part B-Polymer Physics* 41(17) (2003) 2079-2089.
- [29] S. Stassi, V. Cauda, G. Canavese, C.F. Pirri, Flexible Tactile Sensing Based on Piezoresistive Composites: A Review, *Sensors* 14(3) (2014) 5296-5332.
- [30] B. Gorissen, W. Vincentie, F. Al-Bender, D. Reynaerts, M. De Volder, Modeling and bonding-free fabrication of flexible fluidic microactuators with a bending motion, *Journal of Micromechanics and Microengineering* 23(4) (2013).
- [31] F. Connolly, P. Polygerinos, C.J. Walsh, K. Bertoldi, Mechanical Programming of Soft Actuators by Varying Fiber Angle, *Soft Robotics* 2(1) (2015) 26-32.